Article ID: 1000-7032(2022)07-1040-12

Upconversion-bismuth Nanosystem as Theranostic Agent for NIR Laser-driven Chemo-photothermal Therapy

TU Gang[1,2], LING Dan-ping[1,2], LIU Jie[3], WANG Feng[1,2], WANG Hai-fang[3], SHI Li-yi[1,2*], SUN Li-ning[1,2*]

(1. *Research Center of Nano Science and Technology, College of Sciences, Shanghai University, Shanghai* 200444, *China*;
2. *Department of Chemistry, College of Sciences, Shanghai University, Shanghai* 200444, *China*;
3. *Institute of Nanochemistry and Nanobiology, Shanghai University, Shanghai* 200444, *China*)

* *Corresponding Authors, E-mail: shiliyi@shu. edu. cn; lnsun@shu. edu. cn*

Abstract: A hybrid nanosystem of upconversion-bismuth integration (denoted as UBDAs) is designed and synthesized for near infrared (NIR) light-driven chemo-photothermal therapy. The obtained UBDAs present excellent photothermal conversion capacity (~28. 5%) and good biocompatibility. Meanwhile, under excitation of NIR, UBDAs can emit ultraviolet/visible light, which promotes the continuous rotation-flip movement of the photosensitizer azobenzene in the mesoporous, thereby achieving the controlled drug release and avoiding the side effects of traditional ultraviolet light excitation on biological tissues. Photothermal experiments show that UBDAs hybrid nanosystems have a good photothermal effect under 980 nm laser irradiation. In addition, based on Tm^{3+} and Bi element the UBDAs are expected to be used in upconversion luminescence and X-ray computed tomography (CT) imaging to achieve dual-mode imaging-mediated and single NIR-driven chemotherapy and photothermal therapy. Therefore, this work provides a new idea for the integration of diagnosis and synergistically enhanced antitumor therapy.

Key words: upconversion luminescence; imaging; photothermal therapy; drug release; hybrid nanosystems
CLC number: O482. 31 **Document code**: A **DOI**: 10. 37188/CJL. 20220142

用作近红外光引导的化学-光热协同治疗的上转换-铋纳米诊疗剂

涂 港[1,2], 凌丹萍[1,2], 刘 杰[3], 汪 丰[1,2], 王海芳[3], 施利毅[1,2*], 孙丽宁[1,2*]

(1. 上海大学理学院 纳米科学与技术研究中心, 上海 200444;
2. 上海大学理学院 化学系, 上海 200444; 3. 上海大学 纳米化学与生物学研究所, 上海 200444)

摘要: 设计并合成了一种用于近红外光驱动的化学-光热治疗的上转换-铋纳米体系诊疗剂(UBDAs),其具有出色的光热转换能力(28.5%)和良好的生物相容性。同时,在 980 nm 近红外光的激发下,UBDAs 能够发射紫外/可见光,用于促进光敏剂偶氮苯在介孔中的连续旋转-翻转运动,从而实现药物的可控释放,且利用近红外光激发能够有效避免传统紫外光对生物组织的副作用。光热实验表明,UBDAs 杂化纳米体系在 980 nm 激光照射下具有良好的光热效应。此外,含有 Tm^{3+} 和 Bi 元素的 UBDAs 有望用于上转换发光成像和 X 射线计算机

收稿日期: 2022-04-18; **修订日期**: 2022-04-28
基金项目: 国家自然科学基金(51872183); 上海市教育委员会和上海市教育发展基金会"曙光计划"(19SG38)资助项目
Supported by National Natural Science Foundation of China(51872183); "Shuguang Program" Supported by Shanghai Education Development Foundation and Shanghai Municipal Education Commission(19SG38)

断层成像,进而实现双模成像介导且单一近红外光激发的癌症化学疗法和光热疗法。该研究结果为诊断和协同增强抗肿瘤治疗的综合研究提供了新的思路。

关　键　词: 上转换发光; 成像; 光热治疗; 药物释放; 杂化纳米体系

1　Introduction

Because of its high efficiency, low invasion, and remote controllability, photothermal therapy is regarded as one of the most promising therapeutic strategies for antitumor therapy. However, long-term chemotherapy has caused serious toxic and side effects on biological specimens and living tissues, which has brought great difficulties to treatment. It is well known that synergistic treatment has achieved remarkable results in the treatment of various diseases. Therefore, it is necessary to combine other treatments with chemotherapy to achieve synergistic effect in order to overcome the shortcomings of chemotherapy[1].

Photothermal therapy (PTT) causes irreversible damage to tumor tissue and produces good therapeutic effects owing to its advantages, such as non-invasive, high selectivity, and deep penetration depth in biological therapy[2]. In photothermal therapy, near-infrared (NIR) laser energy can be absorbed by the photothermal agent and converted into heat, causing the death of tumor cells[3]. Up to now, noble metal nanoparticles (Au, Pd, and Pt, *etc.*)[4-6], metal chalcogenide compounds, transition metal disulfides[7-9] and carbon nanomaterials, *etc.* have been demonstrated as promising photothermal agents for cancer treatment[10]. However, most of them have the disadvantages of high price, toxicity, and complicated preparation process. Therefore, developing photothermal reagents with low-cost, non-toxic, and environmentally friendly synthetic routes has become one of the hot research spots[11].

Bismuth (Bi) is a heavy metal element with a high atomic number (Z=83) and has a good X-ray attenuation coefficient (5.74 $cm^2 \cdot g^{-1}$, 100 keV)[12]. More importantly, compared with other noblemetals (Au, Pd, and Pt, *etc.*), Bi has the advantages of nontoxicity and low cost, and Bi is an inexpensive "green" metal as well[13]. Moreover, Bi shows a good photothermal conversion ability with a strong NIR absorption capacity. As well known, the long-wavelength NIR light displays better tissue-penetrating capability due to its high maximum permissible exposure and fine spatio-temporal resolution, also provides many possibilities for tumor therapy with improved effectiveness, especially in PTT. Therefore, the nanomaterials based on Bi that triggered by NIR light are expected to be potential photothermal therapy agents[14-15].

Among the reported candidate materials for optical imaging, rare-earth doped upconversion nanoparticles (UCNPs) have been widely used as imaging agents in tumor diagnosis due to their unique optical properties[16-25]. UCNPs can convert NIR light into ultraviolet light, visible light, or NIR light through anti-Stokes displacement. In addition, the hollow mesoporous-type nanocarriers can be used as light-responsive drug carriers, which have many advantages, such as low drug loading rate and good biocompatibility. The photomechanical azobenzene can create a continuous rotation-inversion movement under the upconverted UV/visible light that emitted by UCNPs, thereby achieving a photo-responsive controlled drug release to biological tissues[1,17].

Recent progress on the role of upconversion nanoparticles in cellular therapy suggests that its viability not only as a stimulator and *in vivo* imaging probe, but more importantly, as a real-time monitor of cellular treatments[16-17]. Here, we develop a dual-mode (upconversion luminescence and CT) imaging-mediated and single NIR laser-driven theranostic agent for chemo-photothermal therapy. The final UBDAs exhibit good biocompatibility, and the single NIR laser responsive photothermal and drug-releasing properties were studied. Moreover, the live/dead cell staining assay was performed, demonstrating the effective tumor ablation through synergistic

chemo-photothermal therapy.

2 Experiment

2.1 Materials

Rare-earth chlorides $RECl_3 \cdot 6H_2O$ (99.99%) (*RE*=Y, Yb, Tm), 1-octadecane(90%), and oleic acid (OA, 90%), polyvinyl pyrrolidone (PVP) (99%), hexadecyl trimethyl ammonium bromide (CTAB, 99%), tetraethyl orthosilicate(TEOS), 3-amino-propyl trimethoxysilane(APTES, 98%), and 4-phenyl-azobenzoyl chloride(AZO, 99.9%)were bought from Sigma-Aldrich Co., Ltd. Methanol(CH_3OH, 99.5%), Sodium borohydride($NaBH_4$, 98%), Bismuth nitrate ($Bi(NO_3)_3 \cdot 5H_2O$, 99%), dimethyl sulfoxide(C_2H_6OS, 99.8%), ammonium fluoride(NH_4F, 98%), and sodium hydroxide(NaOH, 96%) were obtained from Aladdin Company. Doxorubicin hydrochloride(98%) was obtained from Jingchun Biotech Co., Ltd. Cyclohexane(C_6H_{12}, 99.7%), ethanol(C_2H_6O, 99.7%) were purchased from Sinopharm Co., Ltd. Ultrapure deionized water(Millipore system) was used for all experiments.

2.2 Synthesis of Bi-PVP Ultra-small Nanoparticles

Bi-PVP was synthesized according to the previous report with minor modification[13]. Bismuth nitrate(0.1 g) and PVP(0.3 g) were added to a solution containing 10 mL of glycerol and 5 mL of ethanol, heated to 60 ℃, and stirred for 1 h. Sodium borohydride(0.05 g) was quickly added and stirred for 1 min. Bi-PVP ultra-small nanoparticles were collected by centrifugation, washed two times with water and ethanol at 4 ℃, then dispersed in ultrapure water(10 mL).

2.3 Synthesis of Mesoporous Silica-coated Upconversion Luminescent Nanomaterials (Denoted as UB@$mSiO_2$)

The $NaYF_4$: 20%Yb, 0.5%Tm (UCNPs) were obtained according to our previous method[25]. 2 mL of UCNPs, 0.1 g of CTAB and 20 mL of deionized water as a surfactant were injected into a small beaker, heated to 60 ℃ and stirred for 1 h, then cooled to room temperature with stirring for 12 h. 40 mL of water, 6 mL of ethanol, Bi-PVP ultra-small nanoparticles, and 150 μL of 2 mol/L sodium hydroxide solution were injected into a 250 mL two-necked bottle connecting with a reflux condenser and continuously stirred at 70 ℃. 200 μL of TEOS was added to the beaker at a constant speed and stirred for 2 h under a reflux condenser[26-27]. The products were centrifugation, washed several times with ethanol, and then dispersed in 10 mL of ethanol. Subsequently, 1.2 g of ammonium nitrate in 190 mL of ethanol was dropped slowly and kept stirring for 12 h at 60 ℃. UB@$mSiO_2$ was collected by centrifugation, washed several times with ethanol, then dispersed in ethanol (10 mL).

2.4 Synthesis of Amino-modified UB@$mSiO_2$ Nanomaterials(Denoted as UB@$mSiO_2$-NH_2)

200 μL of APTES and 15 mL of UB@$mSiO_2$ were injected into a 50 mL flask and stirred for 48 h at 25 ℃. Amino-modified nanomaterials UB@$mSiO_2$-NH_2 were collected by centrifugation, washed several times with ethanol, and then dispersed in ultrapure water(10 mL).

2.5 Synthesis of Hybrid Nanomaterials Loading with DOX(Named as UBDs)

5 mL of DOX (1 mg·mL^{-1} doxorubicin hydrochloride aqueous solution) and 10 mL of UB@$mSiO_2$-NH_2 were injected into a 50 mL flask and stirred for 48 h. The hybrid nanomaterials loaded with DOX were collected by centrifugation, washed several times with ethanol, denoted as UBDs, and then dispersed in dimethyl sulfoxide(DMSO, 10 mL).

2.6 Synthesis of UBDAs Hybrid Nanosystems Encapsulated with AZO (Named as UBDAs)

0.1 g of AZO and 10 mL of UBDs were injected into a 50 mL flask and stirred for 12 h, and the obtained samples were washed with DMSO and absolute ethanol, and then dispersed in 10 mL of ultrapure water, denoted as UBDAs hybrid nanosystems.

2.7 Synthesis of UDAs Hybrid Nanomaterials (Named as UDAs)

UDAs hybrid nanomaterials were synthesized according to the preparation of UBDAs, except that the Bi-PVP was not introduced in synthesis of UB@$mSiO_2$.

2.8 Characterization

A JEM-2100F low-to-high resolution transmission electron microscope (TEM) was used to characterize different morphology at 120 kV. Fourier transform infrared (FTIR) spectra were measured with an Avatar 370 instrument in the spectral range from 4 000 cm^{-1} to 500 cm^{-1}. The upconversion luminescence spectra were acquired using a 980 nm laser with an Edinburgh FS5 fluorescence spectrometer with a 980 nm laser. UV-visible absorption spectra were carried out on a Shimadzu UV-2500PC ultraviolet-visible spectrometer. The zeta potentials were recorded by PCS analysis software on a Nano-ZS (Malvern Instruments Corporation).

2.9 Photothermal Performance

The photothermal effect of the UBDAs was preliminarily evaluated by exposing the corresponding aqueous solutions with various concentrations to a 980 nm laser irradiation (1.5 $W \cdot cm^{-2}$, 10 min)[28-29]. The temperature was recorded using a thermocouple microprobe. To evaluate the photothermal stability, the temperature was measured every 10 s during the five cycles of 10 min laser irradiation and 10 min natural cooling for the aqueous solution of the nanoparticles (UBDAs: 400 $\mu g \cdot mL^{-1}$). The photothermal conversion efficiency (η) was evaluated by recording the temperature variation in a cycle of alternating heating and cooling process[13,30].

2.10 Cell Experiments

HeLa (Human epithelial cervical cancer cell line) was obtained from the Cell Bank of Type Culture Collection of Chinese Academy of Sciences (Shanghai, China). The cells were cultured in high glucose DMEM (4.5 $g \cdot L^{-1}$ glucose) supplemented with 10% (v/v) fetal bovine serum (FBS, Sigma-Aldrich, USA) and 1% penicillin-streptomycin at 37 ℃ and 5% CO_2 in a humidified incubator. HeLa cells were seeded into plates (1×10^4 cells per well in 96-well plates for the live/dead staining, or, 15×10^4 cells per well in 12-well plates for the cell survival) and incubated for 24 h. Subsequently, the cells were exposed to UBDAs for the following assays.

Typan blue staining was used to evaluate the cell survival of the cells treated with the UBDAs. HeLa cells were exposed to the culture medium (10% FBS) containing the UBDAs at different concentrations, and the cells cultured in culture medium without UBDAs as the control[31-32]. After 24 h, the medium was removed, and the typan blue solution (0.4 $mg \cdot mL^{-1}$) was added and cultured for 3 min, where dead cells were stained blue. The cell survival (%) is expressed as the percentage of the surviving cell number of treated groups in that of the control[33-34].

The live/dead staining of cells was conducted by using the kit (L-3224, Invitrogen, USA) following the instruction[35]. The dyes in the kit, Calcein AM and propidium iodide (PI), can differentiate live cells (green, λ_{ex}= 495 nm/λ_{em}= 515 nm) from dead cells (red, λ_{ex}=535 nm/λ_{em}=635 nm). The cells were

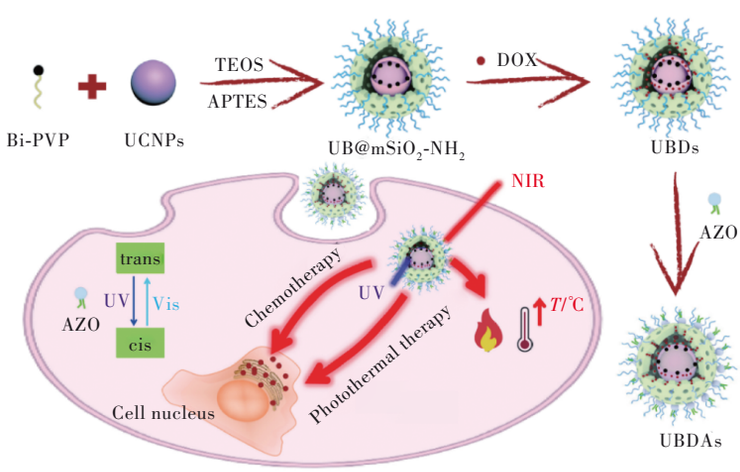

Fig.1　Schematic illustration of designing UBDAs hybrid nanosystem for potential application in synergistically enhanced chemo-photothermal therapy of tumor

cultured in the medium (10% fetal bovine serum) containing 400 μg·mL^{-1} UBDAs for 4 h. The photothermal experimental group was irradiated with 980 nm laser (1.5 W·cm^{-2}) for 10 min. The control group was not treated with laser. After that, the cells were washed with cold D-Hank's solution. The cells were stained with the dyes for 30 min and then observed using a fluorescence microscope.

3 Results and Discussion

3.1 Synthesis and Characterization of UBDAs Hybrid Nanosystem

The design of the UBDAs hybrid nanosystem for synergistically enhanced chemo-photothermal therapy was illustrated in Fig. 1. First, rare earth doped up-conversion luminescence nanoparticles $NaYF_4$:Yb,Tm(UCNPs) and metal bismuth nanoparticles as the core are simultaneously coated in a mesoporous silica shell layer to form a mesoporous coated core-shell hybrid nanosystem UB@mSiO_2 with amino functionalization on the surface, and then loading DOX into mesoporous silica pores. Finally, the drug was encapsulated with AZO compound to obtain the final upconversion-bismuth hybrid nanosystems UBDAs. As shown in Fig. 2, the morphology and structure of the initial UCNPs to the final UBDAs nanosystem were characterized by transmission electron microscopy (TEM). As displayed in Fig. 2(a) and 2(b), the UCNPs show good monodispersity with an average diameter of around 38 nm and Bi-PVP shows a very small size (below 10 nm), respectively.

Fig. 2(c) displays that the SiO_2 mesoporous shell successfully coated on the surface of UCNPs and Bi-PVP, leading to the formation of UB@mSiO_2 with the average size of approximately 55 nm. And from the high-resolution transmission electron microscopy (HR-TEM) image of UB@mSiO_2 in Fig. 2(e), it

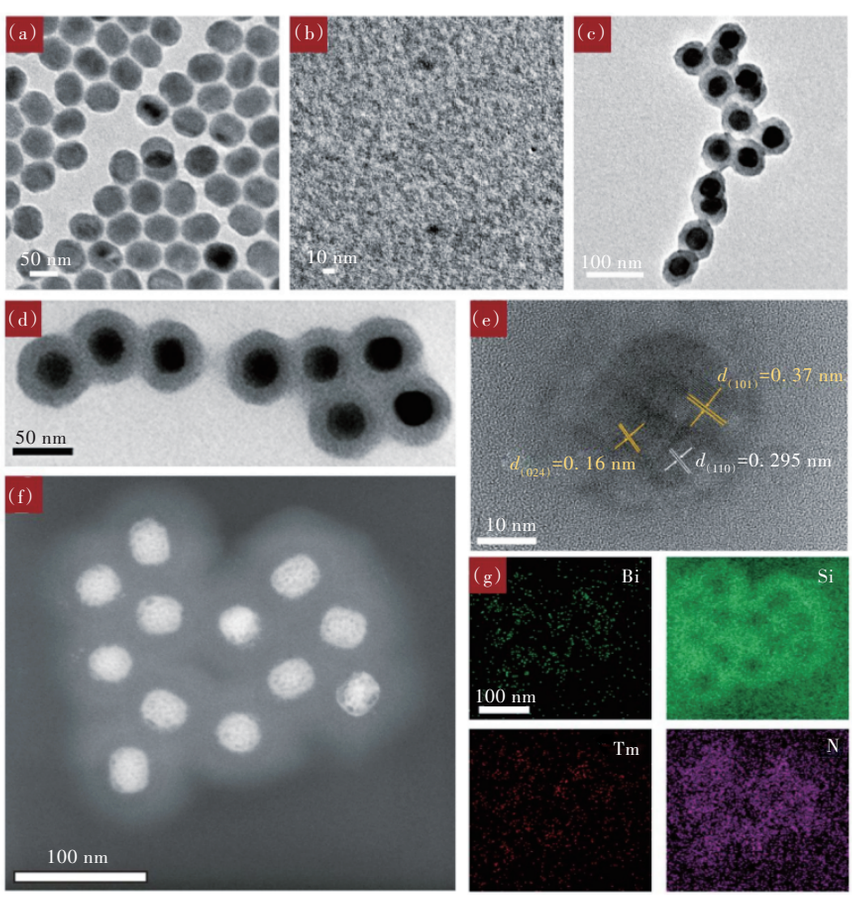

Fig.2 Transmission electron microscope (TEM) images of $NaYF_4$:Yb,Tm(a), Bi-PVP(b), UB@mSiO_2(c), and UBDAs(d). (e) Corresponding high-resolution TEM (HR-TEM) image of UB@mSiO_2. (f)-(g) HAADF-STEM-EDS mapping image of UBDAs.

can be observed that the lattice fringe spacing of 0.295 nm is in agreement with the d-spacing of (110) lattice plane of hexagonal-system $NaYF_4$(JCPDS 16-0334), and 0.37 nm and 0.16 nm are attributed to (101) and (024) of Bi(JCPDS 85-1329), respectively. It can be deduced that the UCNPs and Bi exist in the UB@$mSiO_2$ nanoparticles. From the TEM image(Fig. 2(d)) and HR-TEM image of UBDAs(Fig. 2(f)), it can be observed that there is no obvious increase in particle size of UBDAs after loading with DOX and AZO. From Fig. 2(g), the corresponding elements(Bi, Si, Tm, and N) in the hybrid nanosystem by elemental mapping image suggest that successful synthesis of the UBDAs assemblies by this facile method.

Fig.3(a) shows the zeta potentials of Bi-PVP, UCNPs@$mSiO_2$, UB@$mSiO_2$, UCNPs@$mSiO_2NH_2$, UBDs, and UBDAs nanosystem, respectively. In comparison with the zeta potentials of Bi-PVP and UCNPs@$mSiO_2$ being +38.2 mV and −20.6 mV, respectively, the UB@$mSiO_2$ displays −12.4 mV, indicating that the Bi-PVP was successfully encapsulated in mesoporous silica. After APTES modification, the zeta potential of UB@$mSiO_2$-NH_2 is +45.1 mV, which shows that the —NH_2 group was successfully attached to the UB@$mSiO_2$. The zeta potential of UBDs increases to +47.2 mV, suggesting the successful loading of DOX in UBDs[36]. Since AZO is negatively charged, leading to the zeta potential of UBDAs to be reduced to +23.2 mV, it suggests the successful installing of AZO on UBDs and the formation of UBDAs nanosystem.

Fig. 3(b) shows the FTIR spectra of UCNPs, Bi-PVP, UB@$mSiO_2$, UBDs, and UBDAs nanosystem. In the spectrum of UCNPs, the characteristic peaks at 2 926 cm^{-1} and 2 855 cm^{-1} can be ascribed to the symmetric and asymmetric stretching vibrations of —CH_2 in oleic acid. The two peaks at 1 558 cm^{-1} and 1 465 cm^{-1} are due to the symmetric and asymmetric stretches of —COOH in oleic acid. For the curve of UB@$mSiO_2$, the bands at 1 080 cm^{-1} and 800 cm^{-1} are due to the asymmetric and symmetric vibrations of Si—O—Si, indicating the successful wrapping of mesoporous silica. In the spectrum of

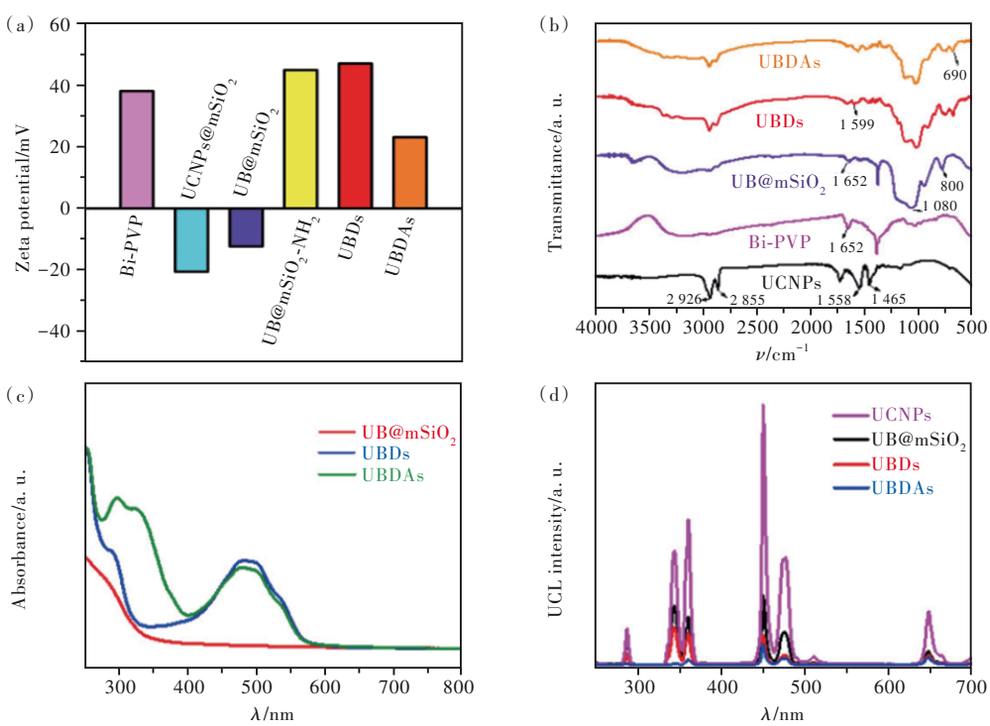

Fig.3 (a)The zeta potentials of Bi-PVP, UCNPs@$mSiO_2$, UB@$mSiO_2$, UB@$mSiO_2$-NH_2, UBDs, and UBDAs dispersed in water(200 μg·mL^{-1}). (b)FTIR spectra of UCNPs, Bi-PVP, UB@$mSiO_2$, UBDs, and UBDAs. (c)UV-visible absorption spectra of UB@$mSiO_2$, UBDs, and UBDAs. (d)Upconversion luminescence spectra of UCNPs, UB@$mSiO_2$, UBDs, and UBDAs dispersed in water(200 μg·mL^{-1}) upon excitation of 980 nm.

UBDs, the peak at 1 599 cm^{-1} is attributed to the stretching vibration of —N—H in the amino-modified silica shell and the amino group of DOX. After AZO was installed, the new peak at 690 cm^{-1} can be attributed to the vibration of benzene ring in the spectrum of UBDAs. Thus, the results above further suggest the formation of UBDAs nanosystem. In addition, Fig. S1 and Fig. S2 show the XRD patterns of Bi-PVP and UBDAs nanosystem. In the pattern of UBDAs, the diffraction peak at a 2θ value of 27.2° is due to the (012) plane of Bi(JCPDS 85-1329), and the diffraction peaks attributed tohexagonal phase of $NaYF_4$(JCPDS16-0334) can be observed as well. The results further indicate that the final nanocomposites are composed of UCNPs and Bi-PVP.

Fig. 3(d) shows the upconversion emission spectra of UCNPs, UB@$mSiO_2$, UBDs, and UBDAs under 980 nm excitation, respectively. The emission peaks located at 291 nm ($^1I_6 \rightarrow {}^3H_6$), 345 nm ($^1I_6 \rightarrow {}^3F_4$), 362 nm ($^1D_2 \rightarrow {}^3H_6$), 450 nm ($^1D_2 \rightarrow {}^3F_4$), 479 nm ($^1G_4 \rightarrow {}^3H_6$), and 648 nm ($^1G_4 \rightarrow {}^3F_4$) belong to the characteristic emission of Tm^{3+} ion. A significant decrease in the upconversion luminescence intensity can be observed in UB@$mSiO_2$ relative to that of UCNPs. It is worth noting that the red emission intensity at 648 nm of UBDs remains almost unchanged, while the emission intensities at 450 nm and 479 nm are reduced in comparison with those of UB@$mSiO_2$. Because of overlap between the green emission of upconversion luminescence and the absorption spectrum of DOX (absorption band with maximum at around 480 nm), the Förster resonance energy transfer(FRET) occurs between UB@$mSiO_2$ and DOX, resulting in green emission of UBDs which was partially diminished after loading of DOX. In addition, the emission peaks at 345 nm and 362 nm of UBDAs, compared with those of UBDs, decrease significantly after AZO is encapsulated. This is because the absorption spectrum of AZO overlaps with the upconversion luminescence spectrum of UBDs in the ultraviolet region(see Fig. 3(c) and 3(d)), leading to FRET between UBDs and AZO. Therefore, the results demonstrate the successful coating of AZO.

3.2 Photothermal Properties

The UBDAs hybrid nanosystem exhibits a broad UV-Vis-NIR absorbance, as shown in Fig. S3, which encourages us to study the potential photothermal property under NIR laser irradiation. The hybrid nanosystem was dispersed in water at different concentrations (50, 100, 200, 400 $\mu g \cdot mL^{-1}$), and pure water was used as the control. As shown in Fig. 4(a), under a 980 nm laser(1.5 $W \cdot cm^{-2}$, 10 min) irradiation the temperatures of UBDAs dispersion raise rapidly with the increase of concentration. The temperature of dispersion at concentration of 200 $\mu g \cdot mL^{-1}$ and 400 $\mu g \cdot mL^{-1}$ increase to 44 ℃ and 52 ℃, respectively, after irradiation for 10 min. However, the temperature of pure water increases by only 3 ℃ after 10 min irradiation. Besides the concentration-dependent photothermal effect, the UBDAs dispersion shows a power-dependent heating effect, and there is a large upward trend with the increase of power densities(0.50, 1.0, 1.5 $W \cdot cm^{-2}$), as shown in Fig S4. The above results indicate that the UBDAs hybrid nanosystem can efficiently convert the NIR light into thermal energy[37]. In addition, the photothermal conversion efficiency(η) is determined to be 28.5% according to the data obtained from Fig. 4(c) and 4(d) by using the reported method[37-39]. The efficiency value is slightly higher in comparison with that of UCNPs@Bi@SiO_2 nanoparticles(28.4%)[40]. To test the photothermal stability, the temperature change of UBDAs dispersion was recorded as a function of time during the five on/off cycles of laser irradiation. As shown in Fig. 4(b), the temperature increment of UBDAs almost maintains unchanged during the heating process after five cycles of irradiation, and the temperature of UBDAs after fifth irradiation is still around 97% of that of the first irradiation, indicating that the UBDAs has good photothermal stability. Furthermore, the infrared thermal images of different concentrations(50, 100, 200, 400 $\mu g \cdot mL^{-1}$) of UBDAs dispersion and pure water are displayed in Fig. 4(e) at the time points of 0, 2, 4, 6, 8, 10 min upon 980 nm laser irradiation(1.5 $W \cdot cm^{-2}$). The UBDAs hybrid nanosystem exhibits notable time-dependent

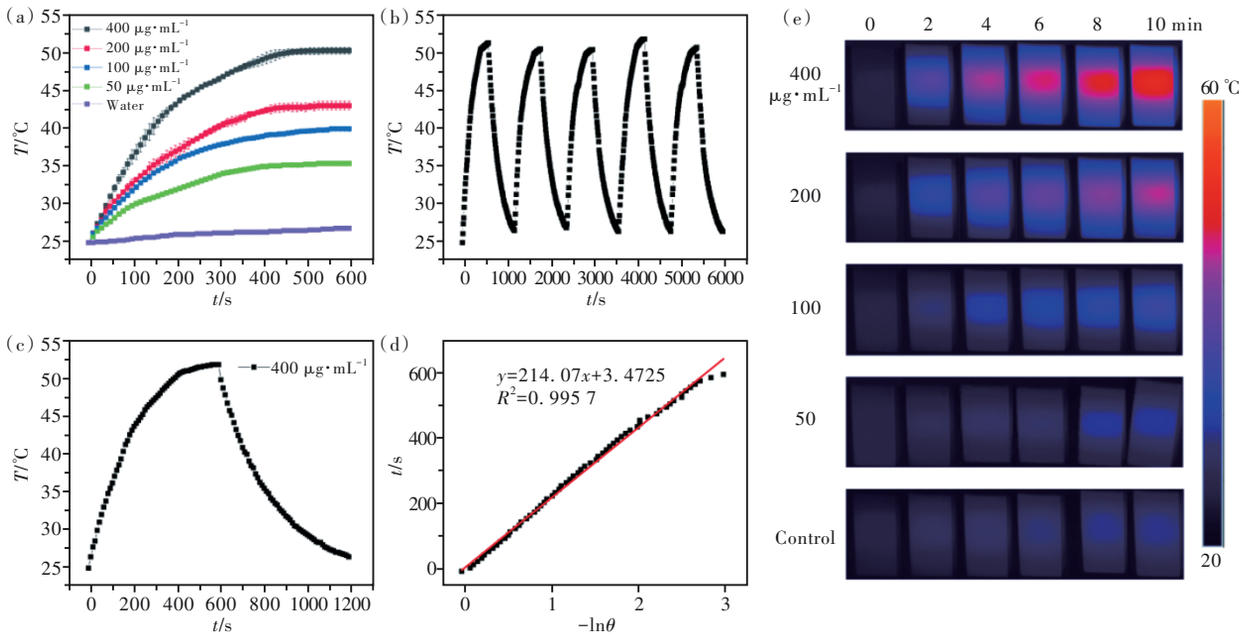

Fig.4　(a)Temperature curves of UBDAs suspensions at various concentrations(50, 100, 200, 400 μg·mL^{-1}) under 980 nm laser(1.5 W·cm^{-2}) irradiation for 10 min. (b)Temperature curves of the UBDAs(400 μg·mL^{-1}) over five cycles of laser on/off operation. (c)Photothermal circulation curves of the UBDAs suspensions. (d)Linear time data *versus* −lnθ obtained from the cooling period of panel Fig.4(c). (e)Infrared thermal images of different concentrations(50, 100, 200, 400 μg·mL^{-1}) of UBDAs hybrid nanosystem and pure water at the time points of 0, 2, 4, 6, 8, 10 min upon 980 nm laser irradiation(1.5 W·cm^{-2}).

and concentration-dependent thermal effects. Since the death of cancer cells can be induced at temperature higher than 42 ℃, the UBDAs hybrid nanosystem is expected to be a potential candidate for PTT of tumor.

3.3　Drug Release

To study the drug release of this nanosystem in response to NIR light, we first tested the absorbance spectra of DOX solution with different concentrations[41-42]. And the absorbance intensity(at 480 nm) as a function of DOX concentration was shown in Fig. 5(a), from which the corresponding standard absorption curve can be simulated and established. Since the photomechanical AZO can create a transformation from *trans*-isomer into *cis*-isomer under UV light excitation[17](Fig. S5), DOX could be released from UBDAs under the upconverted UV light that emitted by UCNPs. Therefore, a photo-responsive controlled DOX release can be achieved from the continuous rotation-inversion movement of AZO depending on the 980 nm laser irradiation on the

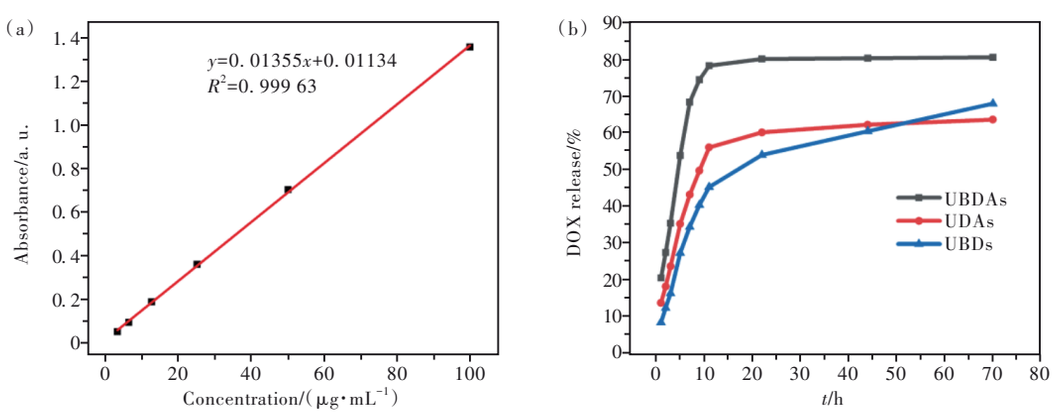

Fig.5　(a)DOX standard curve by testing the absorbance(at 480 nm) of DOX solution with different concentrations(6.25, 12.5, 25.0, 50.0, 100 μg·mL^{-1}). (b)Stimuli-responsive DOX release of UBDAs, UDAs, and UBDs in PBS for 72 h after 980 nm laser(1.5 W·cm^{-2}) irradiation for 10 min.

nanosystem.

Subsequently, the DOX release behaviors of UBDAs, UDAs, and UBDs were further investigated under 980 nm laser irradiation (Fig. 5(b)). From the synthesis process, it is known that UDAs has no Bi being introduced and UBDs has no AZO for encapsulation. As displayed in Fig. 5(b), it can be observed that the release rate of final UBDAs is faster than those of UDAs and UBDs, implying that the photothermal effect of Bi and the *cis-trans* reversal of AZO structure could facilitate the DOX release, respectively. The release of DOX could be triggered by NIR light *via* the *trans*-isomer of AZO. The upconverted UV light emitted by the UCNPs creates a continuous rotation-inversion movement and the back and forth wagging motion of AZO molecules, which acts as a molecular impeller that propels the NIR-triggered release of DOX. Additionally, under 980 nm NIR laser stimuli, the accelerating release of DOX from UBDs (no loading of AZO) also occurs in the PBS solution. This is mainly attributed to the rapid raise of local temperature that induced by the photothermal effect under the laser irradiation, which can enhance the thermal vibration and weaken the interaction between DOX and nanosystem, resulting in the accelerated DOX release.

3.4 *In Vitro* Cytotoxic Effect Against HeLa Cells

Based on the excellent photothermal effect and controllable drug release of UBDAs nanosystem under 980 nm laser irradiation, the nanosystem is considered to be used in the toxicity study of HeLa cells and the effect of photothermal therapy and chemotherapy in killing HeLa cells[43]. Fig. 6 and Fig. S6 show the cell viabilities after the HeLa cells were co-incubated with different concentrations of UBDAs and UB@mSiO_2 for 24 h, and HeLa cells incubated with PBS are used as a blank control group. It can be observed that even at the highest concentration of UBDAs (400 μg·mL^{-1}), the cell survival remains above 95%. This indicates that the nanosystem has low or no cytotoxicity to HeLa cells in the dosages range studied. Thus, the good biocompatibility and photothermal effect as well as the controllable drug release make the nanosystem potentially useful in synergistic photothermal therapy and chemotherapy for cancer cells in biomedical application.

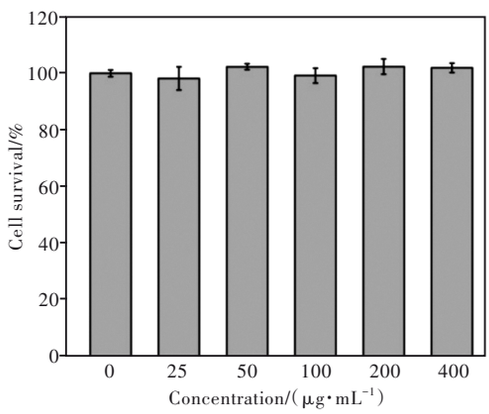

Fig.6 HeLa cells survival after culturing in the medium containing UBDAs with different concentrations (0, 25, 50, 100, 200, 400 μg·mL^{-1}) for 24 h

Encouraged by the high biocompatibility, outstanding photothermal conversion capacity and controllable drug release of the UBDAs nanosystem, the antitumor performance of the nanosystem was evaluated by the live/dead cell staining assay. It is evident from Fig. 7 that UBDAs (400 μg·mL^{-1}) do not affect the viability of the cells in the high concentration because all of the HeLa cells show bright green fluorescence. When HeLa cells were incubated with UBDAs as well as with NIR laser irradiation, nearly all cells were dead and showed red fluorescence, which effectively illustrates that the good antitumor performance of UBDAs upon 980 nm laser irradiation. The loaded DOX could be released from the UBDAs nanosystem by NIR-triggered release, in which the AZO can create a transformation from *trans*-isomer into *cis*-isomer under UV light that generated by the upconversion nanoparticles of the nanosystem. Simultaneously, local temperature raise rapidly that induced by the photothermal effect under the NIR laser irradiation, resulting in the accelerated DOX release. Therefore, the designed UBDAs can be used as the promising single NIR-light stimuli-responsive drug release and photothermal therapy.

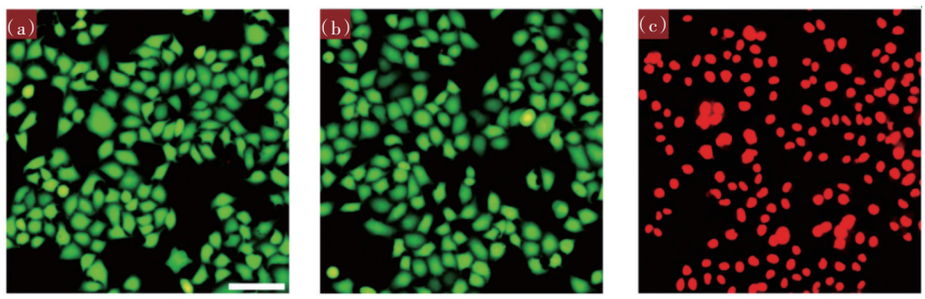

Fig.7　Calcein AM/PI staining images of HeLa cells after incubation with UBDAs(400 μg·mL^{-1}) for 24 h with or without NIR laser irradiation(1.5 W·cm^{-2}, 10 min). Control: HeLa cells incubation with DMEM cell culture medium supplemented with 10%(*v/v*) fetal bovine serum. Scale bar is 100 μm.

4　Conclusions

In summary, a new upconversion-bismuth hybrid nanosystem UBDAs was successfully developed through a mild method, which can be expected to achieve for single NIR-light stimuli-responsive drug release and photothermal therapy. The upconverted UV light emitted by the UCNPs creates a continuous rotation-inversion movement that propels the NIR-triggered release of DOX. More importantly, the UBDAs exhibit extremely high biological safety and effective chemo-photothermal therapy *in vitro*. Therefore, this work opens an opportunity of exploring the new type of hybrid nanosystem for efficiently synergistic tumor therapy.

Supplementary Information and Response Letter are available for this paper at: http://cjl.lightpublishing.cn/thesisDetails#10.37188/CJL.20220142.

References:

[1] HOU B B, YANG W T, DONG C H, *et al*. Controlled co-release of doxorubicin and reactive oxygen species for synergistic therapy by NIR remote-triggered nanoimpellers [J]. *Mater. Sci. Eng.* C-*Mater. Biol. Appl.*, 2017, 74: 94-102.

[2] THAKUR M K, GUPTA A, GHOSH S, *et al*. Graphene-conjugated upconversion nanoparticles as fluorescence-tuned photothermal nanoheaters for Desalination [J]. *ACS Appl. Nano Mater.*, 2019, 2(4): 2250-2259.

[3] KUMAR B, MURALI A, MATTAN I, *et al*. Near-infrared-triggered photodynamic, photothermal, and on demand chemotherapy by multifunctional upconversionnanocomposite [J]. *J. Phys. Chem.* B, 2019, 123(17): 3738-3755.

[4] HE Y C, NIU K, LUO L, *et al*. Reduction and protection: one-step synthesis of polydopamine-coated silver nanowires with superior biosafety for cancer treatment [J]. *ACS Sustainable Chem. Eng.*, 2019, 7(24): 20102-20106.

[5] LIU Y, DING L, WANG D, *et al*. Hollow Pd nanospheres conjugated with Ce6 to simultaneously realize photodynamic and photothermal therapy [J]. *ACS Appl. Bio. Mater.*, 2018, 1(4): 1102-1108.

[6] ZHANG H, WANG Y M, ZHONG H, *et al*. Near-infrared light-activated Pt@Au nanorings-based probe for fluorescence imaging and targeted photothermal therapy of cancer cells [J]. *ACS Appl. Bio. Mater.*, 2019, 2(11): 5012-5020.

[7] ZHOU H, CHE L, GUO Z M, *et al*. Bacteria-mediated ultrathin Bi_2Se_3 nanosheets fabrication and their application in photothermal cancer therapy [J]. *ACS Sustainable Chem. Eng.*, 2018, 6(4): 4863-4870.

[8] ZHANG HH, CHEN G H, YU B, *et al*. Fabrication of PEGy lated Bi_2S_3 nanosheets as a multifunctional platform for multimodal diagnosis and combination therapy for cancer [J]. *ACS Appl. Bio. Mater.*, 2019, 2(9): 3870-3876.

[9] HUANG Y, HUANG J Q, JIANG M Y, *et al*. NIR-triggered theranostic Bi_2S_3 light transducer for on-demand NO release and synergistic gas/photothermal combination therapy of tumors [J]. *ACS Appl. Bio. Mater.*, 2019, 2(11): 4769-4776.

[10] ZHANG M, WANG W T, CUI Y J, *et al*. Magnetofluorescent carbon quantum dot decorated multiwalled carbon nanotubes for dual-modal targeted imaging in chemo-photothermal synergistic therapy [J]. *ACS Biomater. Sci. Eng.*, 2018, 4(1): 151-162.

[11] XUAN Y, YANG XQ, SONG ZY, *et al*. High-security multifunctional nano-bismuth-sphere-cluster prepared from oral

gastric drug for CT/PA dual-mode imaging and chemo-photothermal combined therapy *in vivo* [J]. *Adv. Funct. Mater.*, 2019,29(18):1900017-1-12.

[12] YU X J, LI A, ZHAO C Z, *et al*. Ultrasmall semimetal nanoparticles of bismuth for dual-modal computed tomography/photoacoustic imaging and synergistic thermoradiotherapy [J]. *ACS Nano*, 2017,11(4):3990-4001.

[13] LEI PP, AN R, ZHANG P, *et al*. Ultrafast synthesis of ultrasmall poly(vinylpyrrolidone)-protected bismuth nanodots as a multifunctional theranostic agent for *in vivo* dual-modal CT/photothermal-imaging-guided photothermal therapy [J]. *Adv. Funct. Mater.*, 2017,27(35):1702018-1-10.

[14] SONG Y, LIU G X, DONG X T, *et al*. Au Nanorods@$NaGdF_4$/Yb^{3+}, Er^{3+} multifunctional hybrid nanocomposites with upconversion luminescence, magnetism, and photothermal property [J]. *J. Phys. Chem.* C, 2015,119(32):18527-18536.

[15] HUANG Y, XUE Z L, ZENG S J. Hollow mesoporous Bi@PEG-FA nanoshell as a novel dual-stimuli responsive nanocarrier for synergistic chemo-photothermal cancer therapy [J]. *ACS Appl. Mater. Interfaces*, 2020,12(28):31172-31181.

[16] SUN L N, WEI R Y, FENG J, *et al*. Tailored lanthanide-doped upconversion nanoparticles and their promising bioapplication prospects [J]. *Coord. Chem. Rev.*, 2018,364:10-32.

[17] WANG K P, WU Q, WANG X C, *et al*. Near-infrared control and real-time detection of osteogenic differentiation in mesenchymal stem cells by multifunctional upconversion nanoparticles [J]. *Nanoscale*, 2020,12(25):10106-10116.

[18] 董娅慧, 于佳酩, 王士鹏, 等. β-$NaGdF_4$:Yb^{3+}, Er^{3+}/纤维素纳米晶胆甾型复合膜制备及光学性能 [J]. 发光学报, 2021,42(12):1882-1890.
DONG Y H, YU J M, WANG S P, *et al*. Preparation and optical properties of β-$NaGdF_4$:Yb^{3+}, Er^{3+}/cellulose nanocrystalline cholesteric composite films [J]. *Chin. J. Lumin.*, 2021,42(12):1882-1890. (in Chinese)

[19] 赵皎印, 索浩, 李磊朋, 等. 荧光热增强型稀土掺杂上转换发光材料研究进展 [J]. 发光学报, 2021,42(11):1673-1685.
ZHAO J Y, SUO H, LI L P, *et al*. Recent advances in rare-earth doped upconverisonmaterials with thermally-enhanced emissions [J]. *Chin. J. Lumin.*, 2021,42(11):1673-1685. (in Chinese)

[20] 蒙铭周, 张瑞, 法信蒙, 等. Ce^{3+}掺杂对$NaYF_4$:Yb^{3+}, Tm^{3+}纳米粒子上转换发光性能的影响及其荧光温度特性应用 [J]. 发光学报, 2021,42(11):1763-1773.
MENG M Z, ZHANG R, FA X M, *et al*. Effect of Ce^{3+} doping on upconversion luminescence of $NaYF_4$:Yb^{3+}, Tm^{3+} nanoparticles and application of fluorescence temperature characteristics [J]. *Chin. J. Lumin.*, 2021,42(11):1763-1773. (in Chinese)

[21] SUN X K, SUN J, DONG B, *et al*. Noninvasive temperature monitoring for dual-modal tumor therapy based on lanthanide-doped up-conversion nanocomposites [J]. *Biomaterials*, 2019,201:42-52.

[22] ZHOU B S, SUN X L, DONG B, *et al*. Antibacterial PDT nanoplatform capable of releasing therapeutic gas for synergistic and enhanced treatment against deep infections [J]. *Theranostics*, 2022,12(6):2580-2597.

[23] CHEN B T, DONG B, WANG J, *et al*. Amphiphilic silane modified $NaYF_4$: Yb, Er loaded with $Eu(TTA)_3(TPPO)_2$ nanoparticles and their multi-functions: dual mode temperature sensing and cell imaging [J]. *Nanoscale*, 2013,5(18):8541-8549.

[24] QI M L, LI X, SUN X L, *et al*. Novel nanotechnology and near-infrared photodynamic therapy to kill periodontitis-related biofilm pathogens and protect the periodontium [J]. *Dent. Mater.*, 2019,35(11):1665-1681.

[25] LIU H Y, LI J B, HU P F, *et al*. Facile synthesis of Er^{3+}/Tm^{3+} co-doped magnetic/luminescent nanosystems for possible bioimaging and therapy applications [J]. *J. Rare Earths*, 2022,40(1):11-19.

[26] GE X Q, SUN L N, MA B B, *et al*. Simultaneous realization of Hg^{2+} sensing, magnetic resonance imaging and upconversion luminescence *in vitro* and *in vivo* bioimaging based on hollow mesoporous silica coated UCNPs and ruthenium complex [J]. *Nanoscale*, 2015,7(33):13877-13887.

[27] WEI Z W, SUN L N, LIU J L, *et al*. Cysteine modified rare-earth up-converting nanoparticles for *in vitro* and *in vivo* bioimaging [J]. *Biomaterials*, 2014,35(1):387-392.

[28] LIANG X, YE X Y, WANG C, *et al*. Photothermal cancer immunotherapy by erythrocyte membrane-coated black phosphorus formulation [J]. *J. Control Release*, 2019,296:150-161.

[29] XUE Y M, NIU W, WANG M, *et al*. Engineering a biodegradable multifunctional antibacterial bioactive nanosystem for enhancing tumor photothermo-chemotherapy and bone regeneration [J]. *ACS Nano*, 2020,14(1):442-453.

[30] LV R C, JIANG X, YANG F, *et al.* Degradable magnetic-response photoacoustic/up-conversion luminescence imaging-guided photodynamic/photothermal antitumor therapy [J]. *Biomater. Sci.*, 2019, 7(11): 4558-4567.

[31] LIU W L, ZOU M Z, LIU T, *et al.* Cytomembrane nanovaccines show therapeutic effects by mimicking tumor cells and antigen presenting cells [J]. *Nat. Commun.*, 2019, 10: 3199-1-12.

[32] GOEBELER ME, BARGOU R C. T cell-engaging therapies-bitesand beyond [J]. *Nat. Rev. Clin. Oncol.*, 2020, 17(7): 418-434.

[33] HAN X, SHEN S F, FAN Q, *et al.* Red blood cell-derived nanoerythrosome for antigen delivery with enhanced cancer immunotherapy [J]. *Sci. Adv.*, 2019, 5(10): eaaw6870-1-9.

[34] PAN J, HU P, GUO Y D, *et al.* Combined magnetic hyperthermia and immune therapy for primary and metastatic tumor treatments [J]. *ACS Nano*, 2020, 14(1): 1033-1044.

[35] FENG Y, CHEN H D, SHAO B Q, *et al.* Renal-clearable peptide-functionalized Ba_2GdF_7 nanoparticles for positive tumor-targeting dual-mode bioimaging [J]. *ACS Appl. Mater. Interfaces*, 2018, 10(30): 25511-25518.

[36] SUI B Y, LIU X, SUN J. Dual-dunctional dendritic mesoporous bioactive glass nanospheres for calcium influx-mediated specific tumor suppression and controlled drug delivery *in vivo* [J]. *ACS Appl. Mater. Interfaces*, 2018, 10(28): 23548-23559.

[37] GONG Q Y, XING J, HUANG Y J, *et al.* Perylene diimideoligomer nanoparticles with ultrahigh photothermal conversion efficiency for cancer theranostics [J]. *ACS Appl. Bio. Mater.*, 2020, 3(3): 1607-1615.

[38] ZHOU K, QIU X Y, XU L T, *et al.* Poly(selenoviologen) assembled upconversion nanoparticles for low power single NIR light triggered synergistic photodynamic and photothermal antibacterial therapy [J]. *ACS Appl. Mater. Interfaces*, 2020, 12(23): 26432-26443.

[39] CHEN Q, HUANG G J, WU W T, *et al.* A hybrid eukaryotic-prokaryotic nanoplatform with photothermal modality for enhanced antitumor vaccination [J]. *Adv. Mater.*, 2020, 32(16): 1908185-1-10.

[40] ZHAO S, TIAN R R, SHAO B Q, *et al.* Designing of UCNPs@Bi@SiO_2 hybrid theranostic nanoplatforms for simultaneous multimodal imaging and photothermal therapy [J]. *ACS Appl. Mater. Interfaces*, 2019, 11(1): 394-402.

[41] XUE Y M, DU Y Z, YAN J, *et al.* Monodisperse photoluminescent and highly biocompatible bioactive glass nanoparticles for controlled drug delivery and cell imaging [J]. *J. Mater. Chem.* B, 2015, 3(18): 3831-3839.

[42] CAI X J, JIA X Q, GAO W, *et al.* A versatile nanotheranosticagent for efficient dual-mode imaging guided synergistic chemo-thermal tumor therapy [J]. *Adv. Funct. Mater.*, 2015, 25(17): 2520-2529.

[43] ZHANG Y F, WAN Y L, CHEN Y T, *et al.* Ultrasound-enhanced chemo-photodynamic combination therapy by using albumin "Nanoglue"-based nanotheranostics [J]. *ACS Nano*, 2020, 14(5): 5560-5569.

涂港(1997–),男,湖北荆州人,硕士研究生,2019年于湖北大学获得学士学位,主要从事稀土上转换铋纳米体系的研究。

E-mail: tugang@shu. edu. cnt

孙丽宁(1979–),女,山东威海人,博士,教授/研究员,博士生导师,2008年于中国科学院长春应用化学研究所获得博士学位,主要从事稀土发光纳米材料及其生物成像和治疗、稀土杂化多功能材料及其发光机理、防伪和检测应用的研究。

E-mail: lnsun@shu. edu. cn

施利毅(1963–),男,上海人,博士,教授,博士生导师,1999年于华东理工大学获得博士学位,主要从事纳米功能材料形态结构控制及工业化制备和应用技术的研究。

E-mail: shiliyi@shu. edu. cn